A drone-based sampling platform for vertically resolved chemical characterization of aerosol particles using chemical ionization mass spectrometry

Leo Håkansson[1], Epameinondas Tsiligiannis[1], and Cheng Wu[1]

[1]Department of Chemistry and Molecular Biology, University of Gothenburg, Sweden

Correspondence: Cheng Wu (cheng.wu@gu.se)

Abstract.

Aerosol concentrations and chemical composition exhibitsstrong spatial variability within the planetary boundary layer (PBL), driven by dynamic mixing, vertical development, and removal processes. Yet, vertically resolved measurements of particle-phase composition remain scarce. Here we present a drone-based platform for filter sampling of aerosol particles within the PBL, coupled with real-time meteorological sensing (temperature, relative humidity, wind speed and direction). This approach enhances spatial flexibility for targeted particle collection while enabling subsequent semi-online/offline chemical analysis with a chemical ionization time-of-flight mass spectrometer with a Filter Inlet for Gases and AEROsols (FIGAERO-CIMS). We deployed the platform at an urban site, where its meteorological sensors were validated against tower-based measurements and its particle sampling efficiency was benchmarked against a ground-based filter sampler. The sampling efficiency of the drone-based setup is demonstrated to be sufficient even under relatively clean atmospheric conditions ($PM_{2.5}$ ~2 $\mu g\, m^{-3}$), and is consistent with ground-based sampling with negligible interference from flight operations on collection. In addition, the thermal desorption profiles of individual species with the FIGAERO inlet, which offers a direct measurement of the volatility, exhibit high consistency between the drone-based and ground-based setups. Finally, we demonstrate its capability to resolve vertical gradients in aerosol molecular composition during PBL evolution. This study highlights the potential of unmanned aerial vehicle (UAV) based filter sampling to extend the spatial reach of aerosol chemical characterization using advanced mass spectrometry, providing a versatile tool to understand boundary layer dynamics and aerosol formation and evolution.

1 Introduction

Atmospheric aerosols influence the Earth's radiative balance through processes such as cloud formation and direct light-scattering effects. However, many aspects of aerosol formation, transport, and transformation remain poorly quantified and inadequately represented in models (Shrivastava et al., 2017; Rockström et al., 2009; Ramanathan et al., 2001). A significant portion of aerosol loading consists of secondary organic aerosol (SOA) which forms through the oxidation of biogenic and anthropogenic volatile organic compounds (VOCs). The chemical complexity of SOA arises from the diverse oxidation products, which depend on precursor VOC composition, atmospheric oxidant availability, and levels of anthropogenic pollution (Hallquist et al., 2009, 2016). The spatial distribution of aerosol composition and chemistry exhibits significant variability

(Dieu Hien et al., 2019; Liu et al., 2019). Within the planetary boundary layer (PBL), dynamic mixing and vertical development drive spatial variations in aerosol precursors, aging processes, and removal mechanisms. However, direct, height-resolved measurements of particle-phase composition remain limited in scope and versatility. Significant variations in VOCs, oxidants, and pollutant levels, as well as particle phase composition have been observed in altitude intervals from <100 to 100-1000 m, signifying the importance of vertical mixing, boundary layer dynamics, and height-resolved chemistry close to the surface as well as within the PBL (Asher et al., 2021; Leitner et al., 2023). Recently, Jiang et al. (2024) found that the reactivity of the dominant night-time oxidant, the nitrate radical (NO_3•), with VOCs at 10 and 300 m was 0.17 s^{-1} and 0.034 s^{-1} respectively, after the formation of the nocturnal boundary layer. This elucidates the height-dependent oxidation of VOCs, which in turn drives differences in the functionalization of their oxidation products. Further, utilizing a tethered balloon to sample atmospheric particles up to 750 m, Vandergrift et al. (2024) observed that 7.1% and 24% of CHO and CHON, and 29% of all extremely low volatility organics were unique to aloft measurements. This highlights the potential vertical differences in the speciation and degree of oxidation in aerosol particles.

Conventional approaches are generally associated with towers, aircraft, and tethered balloons, however, they are constrained by cost, spatial coverage, and operational flexibility (Dieu Hien et al., 2019; Liu et al., 2019). Unmanned aerial vehicles (UAVs) have emerged as an alternative, facilitating vertical profiling of atmospheric properties such as meteorology, aerosol properties, oxidants, trace gases, and VOCs with improved resolution and accessibility (Mei et al., 2025; Leitner et al., 2023; Miller et al., 2024; Li et al., 2025). A recent review of copter-based approaches highlight conventional approaches as applicable for UAV-based methods (Li et al., 2025). However, UAV-based studies have predominantly focused on greenhouse gases (Leitner et al., 2023; Gålfalk and Bastviken, 2025), non-methane VOCs (Chen et al., 2022; McKinney et al., 2019), and physiochemical properties of aerosol (Zhu et al., 2025), with few applications directed toward the characterization of aerosol chemical composition at the molecular level. As a result, insights into methodologies for UAV-based particle phase measurements for analysis of chemical composition are comparatively few (Borchers et al., 2025).

Mass spectrometry has become a cornerstone technique in atmospheric chemistry, enabling detailed characterization of atmospheric constituents across molecular to bulk scales and spanning a wide volatility range (from fresh high volatility VOCs to highly oxygenated low volatility products). Chemical ionization mass spectrometry (CIMS), in particular, has advanced our understanding of secondary organic aerosol (SOA) (Ehn et al., 2014; Hallquist et al., 2009) and the role of vapor-phase mixtures in SOA formation (McFiggans et al., 2019). However, as CIMS is inherently a gas-phase technique, particle-phase analysis requires prior vaporization. The Filter Inlet for Gases and AEROsols (FIGAERO) (Lopez-Hilfiker et al., 2014; Thornton et al., 2020) addresses this by collecting particles on a filter for subsequent thermal desorption, enabling simultaneous gas- and particle-phase measurements. The thermal desorption profile from particle-phase measurements, and in particular, the desorption temperature (T) at which a compound's signal reaches its maximum (T_{max}) provides additional information on its volatility. While standard online FIGAERO-CIMS operation provides real-time analysis and minimized sample handling artifacts, the heavy weight and power needs of the mass spectrometer restrict it mostly to stationary operation. Offline filter collection, in contrast, offers greater spatial flexibility and lower sampling burden but is limited in time resolution and potential artifacts, e.g. evaporation of semi-volatiles, adsorption of gases, reactions during storage (Cai et al., 2023a).

Here, a drone sampling platform has been developed to enhance the reach of filter-based sampling of aerosol particles within the PBL for both semi-online and offline chemical characterization with FIGAERO-CIMS. During the semi-online approach, filters are collected near the instrument and then analyzed in rapid succession. This combines the high temporal resolution of online sampling with the spatial adaptability of offline methods. Additionally, the platform incorporates sensors for measuring meteorological parameters (T, humidity, wind speed/direction) and a data acquisition system to better capture PBL dynamics in real time and inform decision-making for targeted aerosol sampling. The performance of the platform was assessed at the University of Gothenburg campus, Sweden, utilizing co-located infrastructure including the Atmospheric Science Lab and a rooftop atmospheric measurement tower. We evaluate drone sensors' accuracy against tower-based weather station data, and compared particle collection efficiency across ground-based and drone-based filter sampling systems. Finally, we demonstrate the platform's capability to profile PBL evolution and resolve molecular-level composition of aerosol at different heights.

2 Methods

2.1 Drone sampling platform

The sampling platform (Fig. 1) was developed using the DJI Matrice 350 drone (SZ DJI Technology Co., Ltd., Shenzhen, China). The fully equipped system, including sensors and a sampling setup (approximately 980 g), resulted in a total flight weight of approximately 7.45 kg, allowing for a flight time of 30 min, including battery redundancy for safe landing. The platform was equipped with a sonic anemometer for wind speed and direction (TriSonica Mini (LI-COR Environmental, Lincoln, NE, USA)), sensors for T and relative humidity (RH) (SKS21 (Sparv Embedded, Linköping, Sweden)), and pressure (SKH3 (Sparv Embedded, Linköping, Sweden)). The anemometer was positioned approximately 2.5 rotor radii (80 cm) from the rotors to reduce propeller-induced turbulence while ensuring structural feasibility. Wind speed and direction were measured at 5 Hz using the sonic anemometer, with a resolution of 0.1 m s^{-1}. The T sensor, reporting a resolution of 0.1 °C with a 0.32 s response time. The RH sensor has a resolution of 0.1 % RH with a response time of 0.5 s at 23 °C. Both T and RH sensors were mounted 20 cm from the drone body to minimize interference from onboard heat sources All meteorological data was integrated into the Sparvio (Sparv Embedded, Linköping, Sweden) system and logged at full resolution.

The particles were collected on a 25 mm diameter Mitex^{TM} PTFE filter with a stainless steel filter holder (Sartorius, Germany) via a 40 cm, 4 mm inner diameter stainless steel inlet co-located with the anemometer to minimize spatial lag and avoid potential interference from rotor downwash. In this configuration, no solar radiation shield was used as all tests were made in Nordic cold to mild temperatures with limited direct solar radiation. When operating in warmer environments, the use of a shielded filter holder may be necessary to minimize artifacts related to thermal effects. A comparison of online FIGAERO-CIMS and drone-mounted filter holders is shown in Fig. 1. Aerosol sampling was conducted using a pump (KVP8-KB, Kamoer, China) mounted on a spring-damped PETG 3D-printed mount. Due to restriction by the sampling line and filter, the maximal sampling flow is 4.5 L min^{-1} with 7 diameter mm mm diameter effective sampling area and 8.5 L min^{-1} with 25 mm effective sampling area. We have also used a Leland Legacy pump (SKC Ltd., Dorset, UK), which offers 4.2 L min^{-1} with 25 mm sampling area. The current application of the platform focuses on bulk characterization, thus no size-selective inlet is applied

and the system nominally sampled total suspended particulate (TSP). However, estimations of the transmission efficiency of the inlet (von der Weiden et al., 2009) indicated that larger particles (10 µm in diameter) may suffer losses exceeding 80%, while particles smaller than 2.5 µm are expected to have a transmission efficiency over 95%. In the present platform configuration, these losses primarily occur at the inlet interface, and are largely independent of the downstream inlet architecture. Consequently, similar inlet conditions are expected for the ground-based sampling configuration used for comparisons. The platform design nevertheless allows straightforward integration of size-selective inlets for studies targeting specific research objectives, such as size-resolved chemical composition or health-relevant aerosol fractions.

In the online sampling system, i.e. CIMS coupled with the FIGAERO inlet (Lopez-Hilfiker et al., 2014), particles were collected on the same 25 mm PTFE filter, and restricted within the central 7 mm diameter area by a Teflon™ insert (25 mm OD with 7 mm central through-hole) (Fig. 1b). To ensure uniformity in collection efficiency, a similar Teflon™ insert or an aluminum foil (both 25 mm OD with 7 mm central through-hole) was applied on the top of the filter, matching the effective collection and desorption area of the online FIGAERO system (Fig. 1). Real-time telemetry enabled adaptive sampling and sensor status monitoring. Pump operation was remotely controlled, and activation times were logged. The entire system was powered by the drone's internal battery, avoiding the need for external sources and ensuring uninterrupted operation. Using regulated onboard power also ensures the pump flow rate remains stable during the duration of the flight.

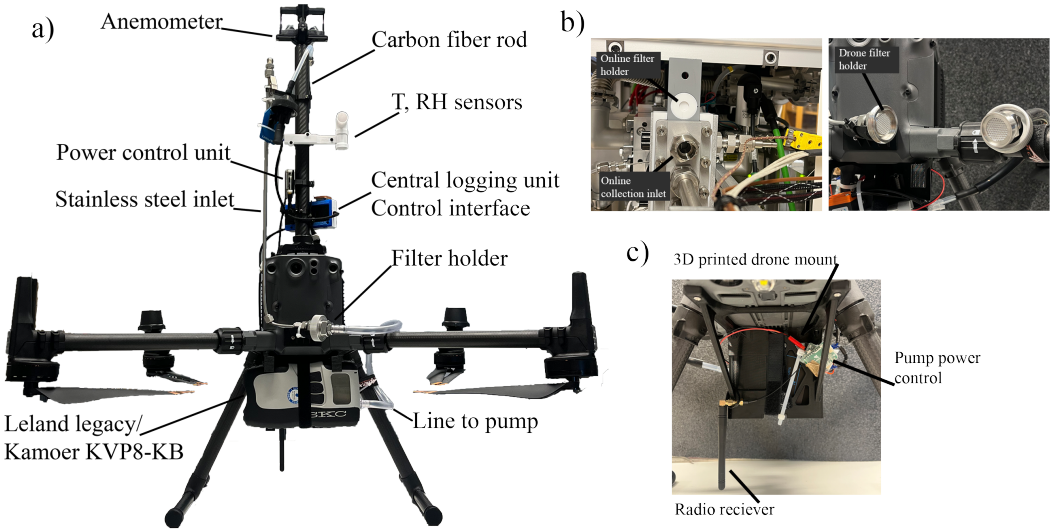

Figure 1. Drone setup overview. (a) Drone platform architecture including sensors, a pump, and a filter holder. (b) Comparison between online filter sampler from the FIGAERO-CIMS and filter holder setup on the drone platform. (c) Underside of the drone including radio receiver placement, 3D-printed drone mount, and pump power control system.

2.2 Particle sampling

For effective online and offline sampling, sufficient particle mass must be collected on the filter, which depends on the ambient particle concentration, and sampling volume (sampling duration × sampling flow rate). In clean environments, higher sampling volume is required, compared to urban and semi-rural settings which typically offer higher mass loading (Thompson et al., 2017). The typical sampling flow of the online FIGAERO-CIMS is 4 – 10 L min^{-1}. With 5 L min^{-1} under ambient aerosol concentrations of 5 μg m^{-3}, the configuration yields a collected mass of 0.75 μg over a sampling duration of 30 minutes. Depending on environmental conditions, the sampling duration can be extended, e.g. to 2–3 hours.

When transferring the method to drone platforms, additional constraints arise from payload capacity and flight endurance. In such cases, pump capacity, i.e maximal sampling flow rate, cannot be indefinitely scaled due to weight limitations. The sampling flow of our system, as mentioned above, is 4.5 L min^{-1} and the collection time could be extended by utilizing a remote-controlled pump that allows pausing sampling during battery swaps. A full stop, landing, battery replacement, and re-ascent cycle can be completed in a few minutes depending on the sampling altitude and desired flight paths, enabling nearly continuous hour-scale collection. When filters are analyzed semi-online, i.e. immediately following collection, sampling durations can be tailored dynamically based on signal strength detected by the CIMS or the organic mass concentration detected by ancillary instrument, such as an aerosol chemical speciation monitor (ACSM). Remote pump control and telemetry enabled strategic spatio-temporal sampling, allowing drone-based filters to be positioned precisely in horizontal or vertical alignment with ground-based systems and meteorological features. After sampling, filters are either transferred directly from the sampler to the FIGAERO inlet for analysis or stored in Petri dishes, wrapped in aluminum foil, and kept at 0°C in a sealed freezer box until analysis (normally within 1–3 hours for semi-online mode).

For offline analysis, the same sampling procedure is applied; however, chemical analysis using the FIGAERO-CIMS is conducted in the lab days to months after sampling collection. While the semi-online mode enables near-real-time characterization of particle chemical composition and allows direct comparison with stationary online measurements, the offline approach increases operational flexibility as it eliminates the need to deploy the mass spectrometer in the field or in a nearby laboratory. However, the offline approach may introduce potential artifacts associated with the potential condensation, re-evaporation, and reactions on the filter during storage, which may result in both positive and negative sampling biases (Cai et al., 2023a).

2.3 Filter analysis with FIGAERO-CIMS

FIGAERO-CIMS provides chemical molecular characterization of aerosol particles. It operates on the principle of filter preconcentration followed by thermal desorption to enable ion-molecule adduct (here iodide as reagent ion) formation of particulate constituents. In online mode, simultaneous filter collection and gas-phase analysis allows for pseudo-continuous, parallel gas- and particle-phase measurements (Lopez-Hilfiker et al., 2014; Thornton et al., 2020).

Adapting FIGAERO-CIMS to offline mode (only particle-phase) involves collecting particles onto filters that are subsequently placed in the FIGAERO filter holder for thermal desorption (Fig. 1). This approach has been previously characterized

and demonstrates good analytical reproducibility (Cai et al., 2023a). Filter collected by the drone can be analyzed at will, either in a semi-online mode (immediately after sampling) or in an offline mode, i.e. at a later stage.

The analysis procedure using FIGAERO-CIMS is identical for both semi-online and offline modes. Filters undergo a desorption cycle: a 20-minute T ramp from room T to 200°C, followed by a 20-minute soak at 200°C, and a 12-minute cooldown. When collecting two simultaneous filters (e.g. one from the drone platform and one from the ground-based sampler), the second is offset by 52-minute, i.e one full desorption cycledesorption of the second filter is started immediately following the first. FIGAERO-CIMS data was processed using the Tofware software package (ToFware 4.0.3, Aerodyne Research Inc., Massachusetts, US) within the Igor Pro v9.0.5. environment (Wavemetrics, Inc., Oregon, US). From the filters collected during this campaign, 303 peaks were assigned at a mass resolution of ~4000 m/Δm. Instrument background was quantified by running clean filters before each analysis segment and was subsequently removed individually for all identified compounds. Then, the background corrected thermograms were integrated, generating the total amount of ions for the full T ramp and soak (first 40 min of the cycle). This integrated signal was then normalized by the sampling volume for further comparison. In addition, the desorption T at which a compounds signal reaches its maximum (T_{max}) was extracted from the thermograms for each assigned peak (Bannan et al., 2019). A detailed description of the instrument operation and data analysis is provided in our previous studies (Salvador et al., 2021; Li et al., 2024; Graham et al., 2023; Wu et al., 2021).

2.4 Platform validation

Field measurements (Table S1) were performed in Gothenburg, Sweden during April 2024 and April to May 2025, Sweden. Gothenburg is a metropolitan coastal city with relatively low particulate loading (annual $PM_{2.5} < 5$ µg m^{-3} in 2024). Emissions are influenced by traffic, nearby industries, and port activities (Tang et al., 2020), while surrounding greenery provide biogenic VOCs. All measurements were made at the University of Gothenburg Natrium Atmosphere and Climate measurement site (Nat-AC-MS) located 100 meters above sea level (MASL) and 25 meters above ground level (MAGL) in the central southwest of Gothenburg.

The drone platform's ability to perform accurate profiling using the onboard meteorological sensors was evaluated and characterized by comparing to the stationary readings (WXT210 Vaisala Oyj, Helsinki, Finland) at the Nat-AC-MS (Fig.S1). The drone platform hovered parallel to the weather station with intermittent landings to swap batteries. Wind speed, wind direction, T, and RH readings were averaged to 5 and 10 seconds and compared to assess the influence of the drone's rotor-induced turbulence on collection of meteorological data. As the averaging time dictates the spatial resolution of a vertical sounding at a fixed speed, the reduction in uncertainty (i.e. standard deviation) with longer averaging times has implications on the flight pattern. Furthermore, multiple vertical profiles at a speed of 1 ms^{-1} and up to a height of 120 MAGL were conducted during both day and night to assess the drone platform's capability to capture dynamic changes.

To evaluate the possible effects of rotor-induced flow on collection efficiency, filters were collected using the drone-based setup in parallel to a ground-based one. The parallel ground-based sampling system used the same filter holder as the drone-based system and was deployed on the Nat-AC-MS tower. During the first experiment both setups were sampling at a height of 8 m above ground (hovering conditions) and the drone was 10 m horizontally from the tower (Fig. S1) whilst during the

second experiment they were sampling at a height of 2 m above ground (grounded conditions, inactive drone rotors) (see Table S1). These comparisons were made during relatively low ($PM_{2.5}$ ~2 – 4 μg m^{-3}) ambient aerosol concentrations. Drone and ground-based filters were both sampled at 4.5 L min^{-1} for 3 hours, resulting in a particle mass loading of at least 1.6 – 3.2 μg at an estimated $PM_{2.5}$ < 2 – 4 μg m^{-3}. Ambient particle loading was estimated using the publicly available City of Gothenburg monitoring program mass concentration measurements taken in the city center of Gothenburg (TEOM Thermo Fisher Scientific Inc., Waltham, MA, USA). The collected filters were analyzed immediately after sampling.

2.5 Aloft Aerosol Particle Measurements

To showcase the capability of the drone platform to map a dynamic lower boundary layer, we present measurements from a typical early spring night characterized by a strong inversion. Vertical profiles of T, RH, wind speed and wind direction as well as aerosol samples were collected. The filter sampling period was a combination of three 30-minute flights, with a total ~1.5 hours . sampling time. Both ground and drone-based filter collections were started simultaneously when the drone reached 120 MAGL, and were intermittently stopped during descent and re-ascent periods to swap drone batteries. The drone-based filters were analyzed immediately by the FIGAERO-CIMS, followed by the filter collected using the ground-based sampling system. Vertical profiles of T, RH, and wind speed and direction were logged during the drone's ascent to 120 m at a speed of 1 m s^{-1}. Two supplementary vertical profiles of meteorological parameters were obtained before and after the full particle sampling sequence, to a total of 5 profiles. Here, a 5-second average is adopted for data collected vertically at a speed of 1 m s^{-1} which results in a resolution of 5 m.

3 Results and Discussion

3.1 Validation of meteorological sensing

The wind speed and direction measured by the drone platform and the stationary measurements show good agreement over the testing period. Wind speeds during the sampling period ranged from of 1–7 m s^{-1}. The comparison between wind speed measured by the drone during hovering and that from the stationary sensor has a slope of 1.09 and an intercept of 0.3 m s^{-1} (Pearson's correlation coefficient (R) 0.91, root mean square error (RMSE) 0.78 m s^{-1}) based on 5 s averages (Fig. 2). At a 10 s average Pearson's R is increased from 0.91 to 0.93 and RMSE is reduced to 0.74 m s^{-1}, the intercept is reduced to 0.2 m s^{-1}. The overall uncertainty of azimuth and elevation angle is quantified with an RMSE of 11.3° and 7.7° and intercepts of 3.5° and 4.3° respectively. At a 10 s average, the RMSE is reduced to 8.6° and 6.6°, respectively.

As reported in previous studies (Prudden et al., 2019; Thielicke et al., 2021) bias in wind measurements is mainly caused by interference from the rotor down-flush, which is dependent on the drone platform setup, specifically the distance between rotor horizontal plane and anemometer, as well as wind speeds and drone movement, previously characterized as a function of rotor throttle or pitch angle. With a similar configuration, Chen et al. (2026) found that sensor-based wind speed measurements achieved good accuracy for hovering and low-speed vertical movement, however they were not shown to be suitable for

high-speed (>2 m s^{-1}) vertical flight patterns. Alternatively, an attitude-based approach showed good accuracy also for high-speed vertical flight patterns. In both cases, platform configuration significantly affected wind speed readings, highlighting the necessity of configuration specific calibrations. Here, the intercepts and slopes were used for correcting our measurement data.

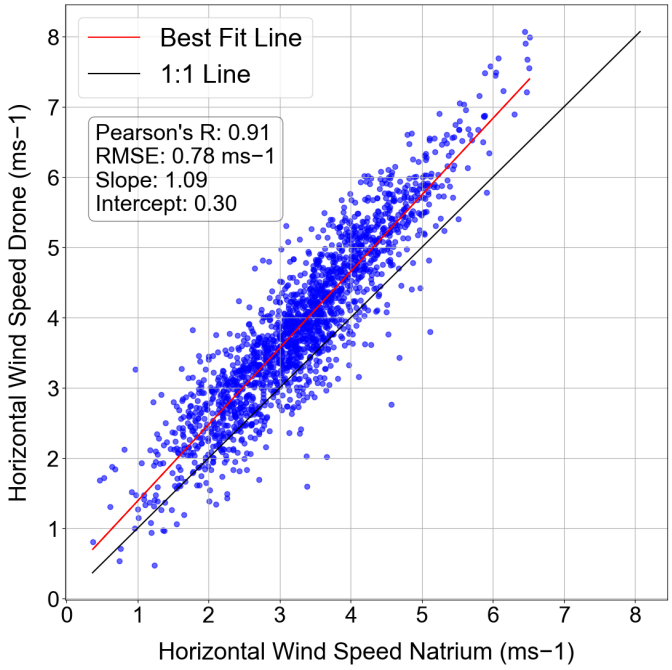

Figure 2. Correlation plot between drone-based and stationary wind speed measurements. 1:1 line in solid black and fitted line in red, data averaged to 5 s.

As presented in Moormann et al. (2025) and Thielicke et al. (2021), a reduction in uncertainty for wind speed and direction can be achieved as averaging time increases. In our case, for both wind speed and direction, increasing the averaging time to 10 seconds does not significantly reduce uncertainties in relation to the trade-off with flight time and desired spatial resolution. Thus, we use a 5 second averaging interval for our following measurements.

T and RH are also important parameters in meteorological sounding as they are commonly used to discern atmospheric stratification (Jiang et al., 2024). T and RH measured during the same testing period exhibited a very good agreement with a slope of 0.98 and 0.97 and intercepts of 0.15 °C and 1.8% for T and RH respectively ((Fig. S3, S4) (RMSE in the order of 0.1 °C and 0.1% RH). Indeed, T and RH sensors infer less uncertainty when mounted on a drone compared to an anemometer. Freeman et al. (2025) evaluated measurement errors of T and water vapor mixing ratio for different unshielded sensor mounting positions on a drone, reporting the largest disagreement with a spread of 0.91 $\mathrm{K} \leq \mathrm{T} \leq 1.88$ K and $-0.22\ \mathrm{g\,kg^{-1}} \leq \mathrm{q}_v \leq 0.66\ \mathrm{g\,kg^{-1}}$ at the sensor placement associated with the highest uncertainty. However, by creating some distance between the sensors and the drone battery as well as avionics, uncertainty could be reduced further. More critical, however, is response time of sensors in

relation to movement speed of the drone, which determines the sensing capability of a drone platform within the desired flight pattern.

The vertical profiles of potential T, specific humidity, wind speed, and wind direction observed during multiple flights over a day-to-night transition period are shown in Fig. 3. Potential T was used here as it is a common parameter used to estimate boundary layer height (Jiang et al., 2024; Baumgartner et al., 2020). Potential T represents the T an air parcel would have when adiabatically brought to a reference pressure (e.g 1000 hPa). As opposed to tracking T, potential T is used to evaluate the atmosphere's actual vertical T gradient, excluding any diabatic change in the probed air. The observed mean potential T per profile dropped significantly from 274 K (min=274.3, max=274.8) at 19:30 to 269 K (min=268.9, max=269.9) at 02:30 (Fig. 3a) and correspondingly water content in the air increased from 2.5 g/kg (min=2.4, max=2.4) at 19:30 to 3.0 g/kg (min=2.9, max=3.1) at 02:30 (Fig. 3b). Variability in profiles of potential T is low (min and max within 0.5 K) between 19:30 and 20:40, however, small but detectable changes at 100 m at 02:30 are observed (min=268.9, max=269.9 K) (Fig. 3a). Which coincides with an enhanced variability in humidity at the same height and time. It is worth noting that interference from the surface (first measurement point represents average and SD from 0 to 5 MAGL) is not significant for all parameters, higher variability can be seen mainly for wind speed and direction, however only in profiles 19:30, 20:40, and 23:30. Wind speed exhibits notable variation between 90 and 110 MAGL at 20:40 which also correlates to relatively large variation of humidity at the same height and time (Fig. 3 b & c). Wind direction exhibits comparatively greater variability at 02:30 specifically between 20 and 50 MAGL (Fig. 3 d). The data collected during descending flights can be potentially poor due to the drone travelling into its own generated downwash, a known issue for drone-based sensor measurements (Li et al., 2025). Thus, only the vertical profiles obtained during ascent were used. In the case that the nocturnal lower boundary layer is more clearly stratified, the first 120 MAGL of the troposphere can exhibit much stronger dynamics (as shown in Fig. 6) than observed in Fig. 3.

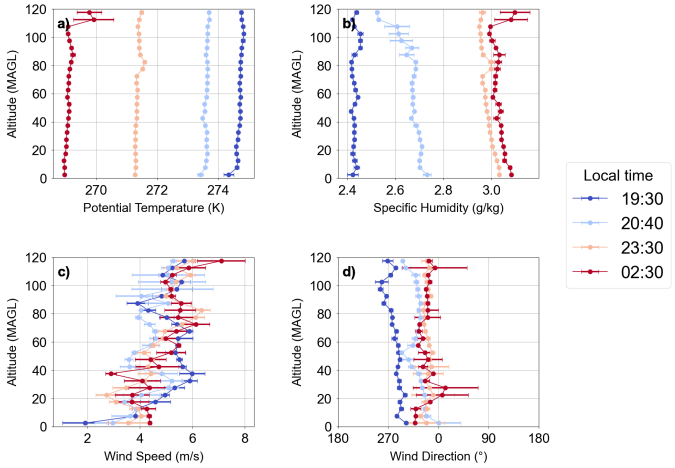

Figure 3. Vertical profiles from test flights of potential T, specific humidity, wind speed, and wind direction up to 120 MAGL between 19:30 and 02:30. Error bars represent the standard deviation.

3.2 Comparison of ground and drone-based sampling setups

In Fig. 4, we present the impacts of drone hovering on sampling with two comparisons: drone inactive (no operations) versus ground-based measurements, and drone hovering versus ground-based measurements. For both conditions, the drone-based and ground-based filter samples show strong agreement with Pearson's R 0.99 and 0.97 for hovering and inactive (i.e. grounded) conditions, respectively. No apparent difference is observed between measurements performed during hovering conditions and while the drone was inactive and grounded, highlighting the negligible rotor-induced perturbations on the collection efficiency and the consistent analytical reproducibility even relatively clean environments. We also notice the uncertainty of the measurement especially for low signal species. While the average differences between drone and ground-based measurements ((|Drone − Ground|)/Ground) for all compounds are 13.4% and 14.1%, for grounded and hovering conditions respectively, the compounds with strong signal have much less relative difference compared to the compounds with weak signals, as demonstrated in Fig. S2. This highlights the necessity of enough particle loading for reliable measurements.

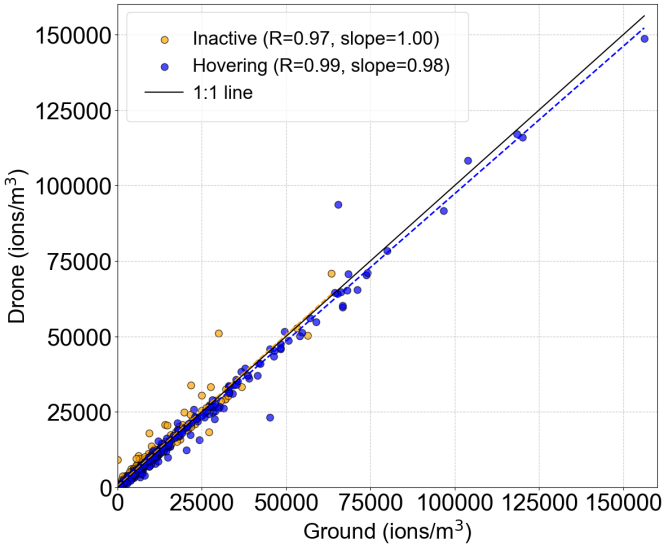

Figure 4. Correlation plot of absolute signal of organic species from drone and ground-based in situ filter collection for 301 organics. Inactive (yellow) where drone was not in flight and hovering (blue) where drone was in flight.

To validate the comparability of drone and ground-based sampling in extracting volatility information, the thermogram shape (the amount of a certain chemical species being desorbed as T increase) and T_{max} of individual compounds from the drone and ground-based filters were compared. T_{max} from the drone-based filter vs ground-based filter shows a good correlation (R = 0.8) with a slope of 0.98 and an intercept of 3 °C. In Fig. 5 four major organic and two major inorganic peaks are shown, area overlap between drone and ground-based thermogram shape is consistently over 92%, with the strongest agreement seen for HNO_3 and $C_7H_{12}O_4$ (agreement >99%). This emphasizes the comparability in volatility information extracted from the drone and ground-based filter collections.

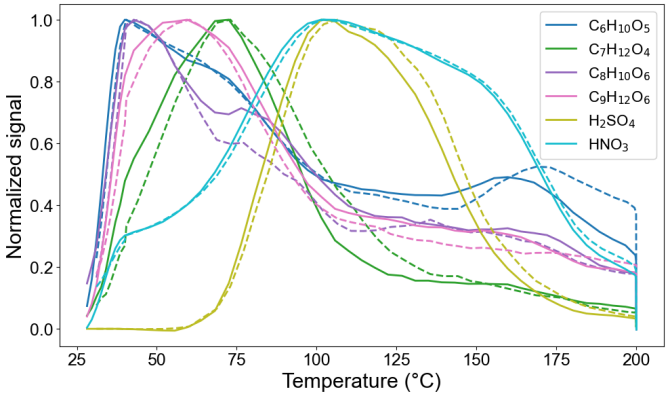

Figure 5. Thermal desorption profiles of selected organic and inorganic compounds from drone-based (solid line) and ground-based (dashed line) filters.

3.3 Vertical profiling of the nocturnal PBL

To demonstrate the drone's ability to detect nocturnal boundary layer dynamics and sample particles aloft, a representative measurement case under stable nocturnal conditions is presented. 5 vertical profiles of wind speed, wind direction, potential T and specific humidity were performed in parallel to ground and drone-based aerosol particle sampling. The vertical profiles revealed a shallow boundary layer as determined by a strong surface-based T inversion (Fig. 6). The potential T increased by approximately 5 K before returning to near stable lapse rate conditions. This indicates stratification of the airmasses based on known boundary layer dynamics (Stull, 1988).

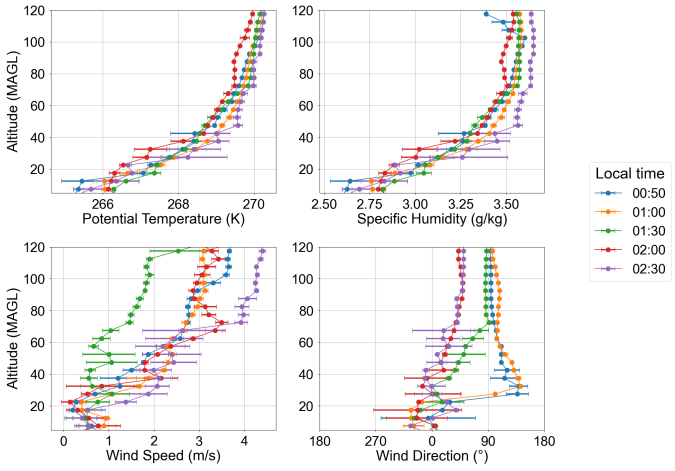

Figure 6. Vertical profile of potential T, specific humidity, wind speed, and wind direction from 00:50 to 02:30 on 15-03-2025 to 120 MAGL.

In contrast to a non-stratified mixed layer, where airmasses transport atmospheric constituents via convective mixing, very little vertical mixing will occur between layers separated by an inversion layer as the coldest air (highest density) is found at the

surface. Hence, sharp differences in particle loading have been observed in relation to T inversion events in different environments and topologies (Glojek et al., 2022; Lei et al., 2021). Here, we observed a significant effect on particle concentration and composition (Fig. 7) due to airmass stratification following the formation of a surface-based inversion layer. The total organic signal is a factor of 3 higher at the ground level compared to aloft. This aligns well with previous studies showing a sharp decline in particulate matter at the height of an inversion layer (Glojek et al., 2022; Lei et al., 2021). Dominant organic species, e.g. $C_5H_8O_4$, $C_9H_{15}NO_6$ and $C_{10}H_{17}NO_7$ are an order of magnitude higher at the ground level. The high signals of nitrated species are consistent with the expectation that nearby NOx emissions during the night are accumulated close to the surface under stable nocturnal boundary-layer conditions (Brown et al., 2013), which lead to formation of organic nitrates from both freshly emitted VOCs and those remaining from daytime emissions (Jiang et al., 2024). The concentration of $C_6H_{10}O_5$ (mainly levoglucosan (Cai et al., 2023b)), a common biomass burning tracer, is also much higher in the ground-based sample. Other potential biomass burning species such as nitrophenol ($C_6H_5NO_3$), methyl nitrophenol ($C_7H_7NO_3$), nitrocatechol ($C_6H_5NO_4$), and methyl nitrocatechol ($C_7H_7NO_4$) are detected in the ground sample at similarly higher concentrations compared to aloft, although not as prominently as levoglucosan. This indicates a potential effect on the dispersion of biomass burning aerosol from the restriction of airmass vertical transport due to the nighttime T inversion. Furthermore, notable inorganic species such as nitric and sulfuric acid (HNO_3, H_2SO_4) are also stratified, with HNO_3 being almost 50% more abundant at the ground level, but H_2SO_4 four times more abundant at 120 m, indicating different source or sink processes.

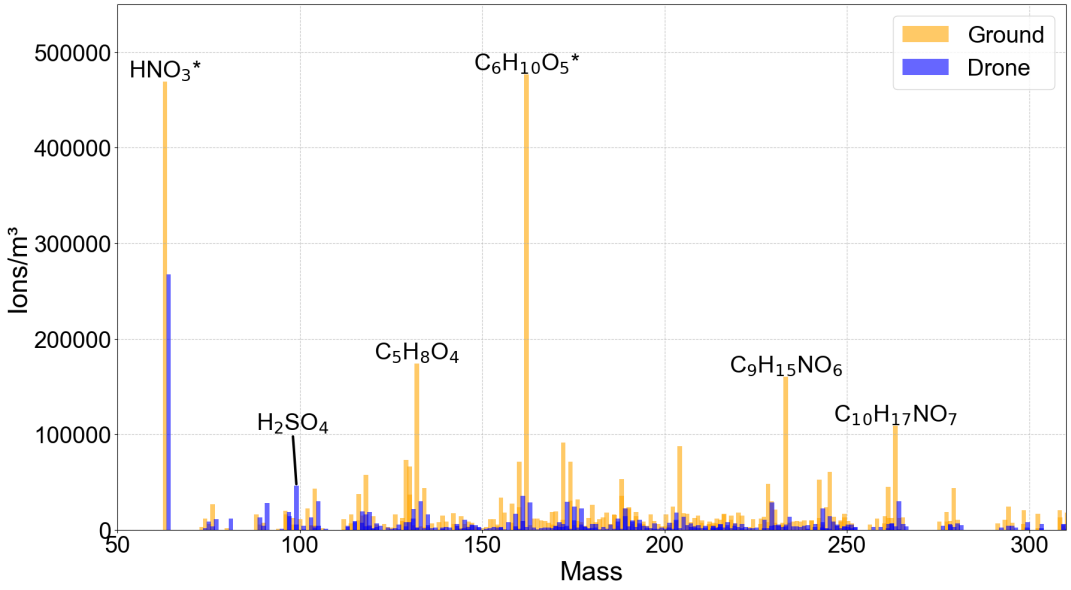

Figure 7. Mass spectra of drone and offline samples. Background subtracted and normalized to collection area and time. Sampled at the same time in parallel to meteorological sounding. *$C_6H_{10}O_5$ reduced by a factor of 2 and HNO_3 was reduced by a factor of 4 to improve visibility.

While nitric acid accumulates at a ground level, sulfuric acid emissions may have different sources, e.g from taller anthropogenic emissions sources and plumes (i.e. emission stacks or scrubber towers). Moreover, comparing the summed thermogram

for ground and aloft measurements reveal a difference in the overall T_{max} by 15 °C from 75°C (ground) to 90°C (aloft). Indicating a lower volatility in aerosol sampled aloft compared at the ground level. More comprehensive results will be presented in our subsequent publication on nocturnal boundary layer chemistry.

3.4 Conclusions

We developed a novel drone platform to sample particulate matter for molecular-level chemical characterization using a FIGAERO-CIMS as well as perform meteorological sensing within the PBL. Following previous work on offline filter collection for FIGAERO-CIMS analysis (Cai et al., 2023a) and many applications in field campaigns (Huang et al., 2024) this platform greatly improves the sampling reach of the instrument. Here, we demonstrated its capability in filter collection and meteorological sounding by validating drone mounted sensors against stationary measurement tower readings, as well as intercomparing ground-based and drone-based filter sampling system.

All sensors (T, RH, and wind speed and direction) displayed good agreement with stationary measurements. Different averaging times, which also relates to the spatial resolution of measurements during in-flight measurements, have been previously documented for similar setups (Moormann et al., 2025). Here, only slight improvements are gained when increasing averaging times from 5 to 10 s. Vertical profiles conducted during the day-to-night transition further demonstrated their good performance, successfully capturing atmospheric changes.

Filter collection efficiency and comparability for the drone and ground-based systems were evaluated by collocated sampling. This comparison for both hovering and inactive conditions showed a very good comparability with negligible effects of drone operation on collection efficiency, highlighting the applicability of drone platforms to perform filter sampling. The comparison of thermograms, i.e volatility information, from drone and ground-based measurements, showed excellent agreement across identified compounds.

Finally, the deployment of the drone platform during nighttime demonstrates its capability to capture vertical gradients in both meteorological parameters and aerosol molecular composition. A surface-based T inversion was detected, where potential T increased by 5 K in the first 120 m AGL. Filter samples collected at the ground and drone level showed significant differences in composition and signal intensity. Total organic signal was higher at the ground level, differing by a factor of 3. Dominant organic species $C_6H_{10}O_5$ (likely levoglucosan), $C_9H_{15}NO_6$ and $C_{10}H_{17}NO_7$ (nitrated monoterpenes) and $C_5H_8O_4$ (oxygenated isoprene product) differed by an order of magnitude. Further, inorganic species such as HNO_3 and H_2SO_4 are also seemingly stratified, where HNO_3 is more abundant at the ground level, and H_2SO_4 is more abundant aloft.

The drone platform presented here offers greatly improved spatial coverage for aerosol particle sampling as compared to the conventional online and offline sampling system. It offers the possibility to sample in otherwise inaccesible locations and altitudes at a low cost and high mobility, improving direct characterization of the vertical variability in aerosol chemical composition. Naturally, the platform is not without its limitations, payload capacity and flight time are constrained by technical progress and filter collection can be challenging in very clean environments. Nevertheless, the platform presented here provides novel insights into drone operation and enabling flexible, extended filter collection, which can be widely applicable and adaptable to other chemical analysis techniques.

4 Author contributions

Conceptualization was done by C.W. and L.H. Data collection was performed by L.H., C.W. and E.T. Data analysis and visualization was done by L.H. Funding was acquired by C.W. Supervision was carried out by C.W. Manuscript writing was done by L.H., with contribution from C.W. and input from E.T. All co-authors contributed to scientific discussions and reviewing the manuscript.

5 Competing interests

The authors declare that they have no conflict of interest.

6 Data availability

All data is available upon request from the corresponding author. Cheng Wu (cheng.wu@gu.se)

7 Acknowledgements

The work was supported by the Swedish strategic research area ModElling the Regional and Global Earth System (MERGE), the Swedish Research Council for Sustainable Development (FORMAS, grant no. 2022-01441, 2024-01102), and Swedish Research Council (grant no. 2024-05576). The authors gratefully acknowledge the support of Mattias Hallquist, principal investigator of the Natrium Atmospheric and Climate Measurement Site (Nat-AC-MS), and the contributions of researchers from the Department of Earth Sciences, University of Gothenburg, led by Fredrik Lindberg, for their efforts in maintaining the stationary meteorological measurements and data collection at Nat-AC-MS.

References

Asher, E., Hills, A. J., Hornbrook, R. S., Shertz, S., Gabbard, S., Stephens, B. B., Helmig, D., and Apel, E. C.: Unpiloted Aircraft System Instrument for the Rapid Collection of Whole Air Samples and Measurements for Environmental Monitoring and Air Quality Studies, Environmental Science & Technology, 55, 5603–6526, https://doi.org/https://doi.org/10.1021/acs.est.0c07213, 2021.

Bannan, T. J., Le Breton, M., Priestley, M., Worrall, S. D., Bacak, A., Marsden, N. A., Mehra, A., Hammes, J., Hallquist, M., Alfarra, M. R., Krieger, U. K., Reid, J. P., Jayne, J., Robinson, W., McFiggans, G., Coe, H., Percival, C. J., and Topping, D.: A method for extracting calibrated volatility information from the FIGAERO-HR-ToF-CIMS and its experimental application, Atmospheric Measurement Techniques, 12, 1429–1439, https://doi.org/10.5194/amt-12-1429-2019, 2019.

Baumgartner, M., Weigel, R., Harvey, A. H., Plöger, F., Achatz, U., and Spichtinger, P.: Reappraising the appropriate calculation of a common meteorological quantity: potential temperature, Atmospheric Chemistry and Physics, 20, 15 585–15 616, https://doi.org/10.5194/acp-20-15585-2020, 2020.

Borchers, C., Moormann, L., Geil, B., Karbach, N., and Hoffmann, T.: Development and use of a lightweight sampling system for height-selective drone-based measurements of organic aerosol particles, EGUsphere, 2025, 1–19, https://doi.org/10.5194/egusphere-2024-4015, 2025.

Brown, S. S., Dubé, W. P., Bahreini, R., Middlebrook, A. M., Brock, C. A., Warneke, C., de Gouw, J. A., Washenfelder, R. A., Atlas, E., Peischl, J., Ryerson, T. B., Holloway, J. S., Schwarz, J. P., Spackman, R., Trainer, M., Parrish, D. D., Fehshenfeld, F. C., and Ravishankara, A. R.: Biogenic VOC oxidation and organic aerosol formation in an urban nocturnal boundary layer: aircraft vertical profiles in Houston, TX, Atmos. Chem. Phys., 13, 11 317–11 337, https://doi.org/10.5194/acp-13-11317-2013, aCP, 2013.

Cai, J., Daellenbach, K. R., Wu, C., Zheng, Y., Zheng, F., Du, W., Haslett, S. L., Chen, Q., Kulmala, M., and Mohr, C.: Characterization of offline analysis of particulate matter with FIGAERO-CIMS, Atmos. Meas. Tech., 16, 1147–1165, https://doi.org/10.5194/amt-16-1147-2023, aMT, 2023a.

Cai, Y., Ye, C., Chen, W., Hu, W., Song, W., Peng, Y., Huang, S., Qi, J., Wang, S., Wang, C., Wu, C., Wang, Z., Wang, B., Huang, X., He, L., Gligorovski, S., Yuan, B., Shao, M., and Wang, X.: The important contribution of secondary formation and biomass burning to oxidized organic nitrogen (OON) in a polluted urban area: insights from in situ measurements of a chemical ionization mass spectrometer (CIMS), Atmos. Chem. Phys., 23, 8855–8877, https://doi.org/10.5194/acp-23-8855-2023, aCP, 2023b.

Chen, D., Su, W., Jiang, S., Yang, H., Zhang, C., Jiang, S., Chang, D., Liang, Y., Wang, H., Yang, X., Fu, T.-M., Zeng, Z., Zhu, L., Shen, H., Wang, C., and Ye, J.: Wind estimation based on flight dynamics of unmanned aerial vehicle: influencing variables and its environmental application, Atmospheric Chemistry and Physics, 26, 3607–3620, https://doi.org/10.5194/acp-26-3607-2026, 2026.

Chen, W., Zou, Y., Mo, W., Di, D., Wang, B., Wu, M., Huang, Z., and Hu, B.: Onsite Identification and Spatial Distribution of Air Pollutants Using a Drone-Based Solid-Phase Microextraction Array Coupled with Portable Gas Chromatography-Mass Spectrometry via Continuous-Airflow Sampling, Environmental Science & Technology, 56, 16 541–17 492, https://doi.org/https://doi.org/10.1021/acs.est.2c05259, 2022.

Dieu Hien, V. T., Lin, C., Thanh, V. C., Kim Oanh, N. T., Thanh, B. X., Weng, C.-E., Yuan, C.-S., and Rene, E. R.: An overview of the development of vertical sampling technologies for ambient volatile organic compounds (VOCs), Journal of Environmental Management, 247, 401–412, https://doi.org/https://doi.org/10.1016/j.jenvman.2019.06.090, 2019.

Ehn, M., Thornton, J. A., Kleist, E., Sipilä, M., Junninen, H., Pullinen, I., Springer, M., Rubach, F., Tillmann, R., Lee, B., Lopez-Hilfiker, F., Andres, S., Acir, I.-H., Rissanen, M., Jokinen, T., Schobesberger, S., Kangasluoma, J., Kontkanen, J., Nieminen, T., Kurtén, T., Nielsen,

L. B., Jørgensen, S., Kjaergaard, H. G., Canagaratna, M., Maso, M. D., Berndt, T., Petäjä, T., Wahner, A., Kerminen, V.-M., Kulmala, M., Worsnop, D. R., Wildt, J., and Mentel, T. F.: A large source of low-volatility secondary organic aerosol, Nature, 506, 476–479, https://doi.org/10.1038/nature13032, 2014.

Freeman, S. W., Bukowski, J., Grant, L. D., Marinescu, P. J., Park, J. M., Hitchcock, S. M., Neumaier, C. A., and van den Heever, S. C.: Characterizing Thermodynamic Observations from Unshielded Multirotor Drone Sensors, EGUsphere, 2025, 1–30, https://doi.org/10.5194/egusphere-2024-2425, eGUsphere, 2025.

Glojek, K., Močnik, G., Alas, H. D. C., Cuesta-Mosquera, A., Drinovec, L., Gregorič, A., Ogrin, M., Weinhold, K., Ježek, I., Müller, T., Rigler, M., Remškar, M., van Pinxteren, D., Herrmann, H., Ristorini, M., Merkel, M., Markelj, M., and Wiedensohler, A.: The impact of temperature inversions on black carbon and particle mass concentrations in a mountainous area, Atmos. Chem. Phys., 22, 5577–5601, https://doi.org/10.5194/acp-22-5577-2022, aCP, 2022.

Graham, E. L., Wu, C., Bell, D. M., Bertrand, A., Haslett, S. L., Baltensperger, U., El Haddad, I., Krejci, R., Riipinen, I., and Mohr, C.: Volatility of aerosol particles from NO3 oxidation of various biogenic organic precursors, Atmos. Chem. Phys., 23, 7347–7362, https://doi.org/10.5194/acp-23-7347-2023, aCP, 2023.

Gålfalk, M. and Bastviken, D.: In Situ Observations Reveal Underestimated Greenhouse Gas Emissions from Wastewater Treatment with Anaerobic Digestion – Sludge Was a Major Source for Both CH4 and N2O, Environmental Science & Technology, 59, 18 146–18 155, https://doi.org/10.1021/acs.est.5c04780, doi: 10.1021/acs.est.5c04780, 2025.

Hallquist, M., Wenger, J. C., Baltensperger, U., Rudich, Y., Simpson, D., Claeys, M., Dommen, J., Donahue, N. M., George, C., Goldstein, A. H., Hamilton, J. F., Herrmann, H., Hoffmann, T., Iinuma, Y., Jang, M., Jenkin, M. E., Jimenez, J. L., Kiendler-Scharr, A., Maenhaut, W., McFiggans, G., Mentel, T. F., Monod, A., Prévôt, A. S. H., Seinfeld, J. H., Surratt, J. D., Szmigielski, R., and Wildt, J.: The formation, properties and impact of secondary organic aerosol: current and emerging issues, Atmos. Chem. Phys., 9, 5155–5236, https://doi.org/10.5194/acp-9-5155-2009, aCP, 2009.

Hallquist, M., Munthe, J., Hu, M., Wang, T., Chan, C. K., Gao, J., Boman, J., Guo, S., Hallquist, Å. M., Mellqvist, J., Moldanova, J., Pathak, R. K., Pettersson, J. B., Pleijel, H., Simpson, D., and Thynell, M.: Photochemical smog in China: scientific challenges and implications for air-quality policies, National Science Review, 3, 401–403, https://doi.org/10.1093/nsr/nww080, 2016.

Huang, W., Wu, C., Gao, L., Gramlich, Y., Haslett, S. L., Thornton, J., Lopez-Hilfiker, F. D., Lee, B. H., Song, J., Saathoff, H., Shen, X., Ramisetty, R., Tripathi, S. N., Ganguly, D., Jiang, F., Vallon, M., Schobesberger, S., Yli-Juuti, T., and Mohr, C.: Variation in chemical composition and volatility of oxygenated organic aerosol in different rural, urban, and mountain environments, Atmos. Chem. Phys., 24, 2607–2624, https://doi.org/10.5194/acp-24-2607-2024, aCP, 2024.

Jiang, S., Wang, Y., Huang, X., Liu, B., Nie, D., Ge, Y., Ma, L., Wang, Q., Wang, J., Ma, Y., Jiang, S., Shu, Z., Zhang, Y., Sun, J., Wu, C., Ge, X., Zhu, L., Shen, H., Wang, C., Zheng, Y., Fu, T.-M., Yang, X., Li, Y. J., Chen, Q., and Ye, J.: Characteristics of Nocturnal Boundary Layer over a Subtropical Forest: Implications for the Dispersion and Fate of Atmospheric Species, Environmental Science & Technology, 58, 23 075–23 087, https://doi.org/10.1021/acs.est.4c05051, doi: 10.1021/acs.est.4c05051, 2024.

Lei, L., Sun, Y., Ouyang, B., Qiu, Y., Xie, C., Tang, G., Zhou, W., He, Y., Wang, Q., Cheng, X., Fu, P., and Wang, Z.: Vertical Distributions of Primary and Secondary Aerosols in Urban Boundary Layer: Insights into Sources, Chemistry, and Interaction with Meteorology, Environmental Science & Technology, 55, 4183–5602, https://doi.org/https://doi.org/10.1021/acs.est.1c00479, 2021.

Leitner, S., Feichtinger, W., Mayer, S., Mayer, F., Krompetz, D., Hood-Nowotny, R., and Watzinger, A.: UAV-based sampling systems to analyse greenhouse gases and volatile organic compounds encompassing compound-specific stable isotope analysis, Atmos. Meas. Tech., 16, 513–527, https://doi.org/10.5194/amt-16-513-2023, aMT, 2023.

Li, L., Thomsen, D., Wu, C., Priestley, M., Iversen, E. M., Tygesen Skonager, J., Luo, Y., Ehn, M., Roldin, P., Pedersen, H. B., Bilde, M., Glasius, M., and Hallquist, M.: Gas-to-Particle Partitioning of Products from Ozonolysis of Δ3-Carene and the Effect of Temperature and Relative Humidity, The Journal of Physical Chemistry A, 128, 918–928, https://doi.org/10.1021/acs.jpca.3c07316, doi: 10.1021/acs.jpca.3c07316, 2024.

Li, Y., Zhang, C., Su, W., Jiang, S., Nie, D., Wang, Y., Wang, Y., He, H., Chen, Q., Martin, S. T., and Ye, J.: Copter-Type UAV-Based Sensing in Atmospheric Chemistry: Recent Advances, Applications, and Future Perspectives, Environmental Science & Technology, 59, 13 532–13 550, https://doi.org/10.1021/acs.est.5c00074, 2025.

Liu, Q., Quan, J., Jia, X., Sun, Z., Li, X., Gao, Y., and Liu, Y.: Vertical Profiles of Aerosol Composition over Beijing, China: Analysis of In Situ Aircraft Measurements, Journal of the Atmospheric Sciences, 76, 231–245, https://doi.org/https://doi.org/10.1175/JAS-D-18-0157.1, 2019.

Lopez-Hilfiker, F. D., Mohr, C., Ehn, M., Rubach, F., Kleist, E., Wildt, J., Mentel, T. F., Lutz, A., Hallquist, M., Worsnop, D., and Thornton, J. A.: A novel method for online analysis of gas and particle composition: description and evaluation of a Filter Inlet for Gases and AEROsols (FIGAERO), Atmos. Meas. Tech., 7, 983–1001, https://doi.org/10.5194/amt-7-983-2014, aMT, 2014.

McFiggans, G., Mentel, T. F., Wildt, J., Pullinen, I., Kang, S., Kleist, E., Schmitt, S., Springer, M., Tillmann, R., Wu, C., Zhao, D., Hallquist, M., Faxon, C., Le Breton, M., Hallquist, A. M., Simpson, D., Bergström, R., Jenkin, M. E., Ehn, M., Thornton, J. A., Alfarra, M. R., Bannan, T. J., Percival, C. J., Priestley, M., Topping, D., and Kiendler-Scharr, A.: Secondary organic aerosol reduced by mixture of atmospheric vapours, Nature, 565, 587–593, https://doi.org/10.1038/s41586-018-0871-y, 2019.

McKinney, K. A., Wang, D., Ye, J., de Fouchier, J.-B., Guimarães, P. C., Batista, C. E., Souza, R. A. F., Alves, E. G., Gu, D., Guenther, A. B., and Martin, S. T.: A sampler for atmospheric volatile organic compounds by copter unmanned aerial vehicles, Atmospheric Measurement Techniques, 12, 3123–3135, https://doi.org/10.5194/amt-12-3123-2019, 2019.

Mei, F., Zhang, Q., Zhang, D., Fast, J. D., Kulkarni, G., Pekour, M. S., Niedek, C. R., Glienke, S., Silber, I., Schmid, B., Tomlinson, J. M., Mehta, H. S., Mansoura, X., Cheng, Z., Vandergrift, G. W., Lata, N. N., China, S., and Zhu, Z.: Measurement report: Vertically resolved atmospheric properties observed over the Southern Great Plains with the ArcticShark uncrewed aerial system, Atmos. Chem. Phys., 25, 3425–3444, https://doi.org/10.5194/acp-25-3425-2025, aCP, 2025.

Miller, A. J., Ramelli, F., Fuchs, C., Omanovic, N., Spirig, R., Zhang, H., Lohmann, U., Kanji, Z. A., and Henneberger, J.: Two new multirotor uncrewed aerial vehicles (UAVs) for glaciogenic cloud seeding and aerosol measurements within the CLOUDLAB project, Atmos. Meas. Tech., 17, 601–625, https://doi.org/10.5194/amt-17-601-2024, aMT, 2024.

Moormann, L., Böttger, T., Schuhmann, P., Valero, L., Fachinger, F., and Drewnick, F.: The Flying Laboratory FLab: development and application of a UAS to measure aerosol particles and trace gases in the lower troposphere, Atmos. Meas. Tech., 18, 1441–1459, https://doi.org/10.5194/amt-18-1441-2025, aMT, 2025.

Prudden, S., Watkins, S., Fisher, A., and Mohamed, A.: A Flying Anemometer Quadrotor: Part 1, 2019.

Ramanathan, V., Crutzen, P. J., Kiehl, J. T., and Rosenfeld, D.: Aerosols, Climate, and the Hydrological Cycle, Science, 294, 2119–2124, https://doi.org/10.1126/science.1064034, doi: 10.1126/science.1064034, 2001.

Rockström, J., Steffen, W., Noone, K., Persson, A., Chapin, F. S., Lambin, E. F., Lenton, T. M., Scheffer, M., Folke, C., Schellnhuber, H. J., Nykvist, B., de Wit, C. A., Hughes, T., van der Leeuw, S., Rodhe, H., Sörlin, S., Snyder, P. K., Costanza, R., Svedin, U., Falkenmark, M., Karlberg, L., Corell, R. W., Fabry, V. J., Hansen, J., Walker, B., Liverman, D., Richardson, K., Crutzen, P., and Foley, J. A.: A safe operating space for humanity, Nature, 461, 472–475, https://doi.org/10.1038/461472a, 2009.

Salvador, C. M. G., Tang, R., Priestley, M., Li, L., Tsiligiannis, E., Le Breton, M., Zhu, W., Zeng, L., Wang, H., Yu, Y., Hu, M., Guo, S., and Hallquist, M.: Ambient nitro-aromatic compounds, biomass burning versus secondary formation in rural China, Atmos. Chem. Phys., 21, 1389–1406, https://doi.org/10.5194/acp-21-1389-2021, aCP, 2021.

Shrivastava, M., Cappa, C. D., Fan, J., Goldstein, A. H., Guenther, A. B., Jimenez, J. L., Kuang, C., Laskin, A., Martin, S. T., Ng, N. L., Petaja, T., Pierce, J. R., Rasch, P. J., Roldin, P., Seinfeld, J. H., Shilling, J., Smith, J. N., Thornton, J. A., Volkamer, R., Wang, J., Worsnop, D. R., Zaveri, R. A., Zelenyuk, A., and Zhang, Q.: Recent advances in understanding secondary organic aerosol: Implications for global climate forcing, Reviews of Geophysics, 55, 509–559, https://doi.org/https://doi.org/10.1002/2016RG000540, 2017.

Stull, R. B.: An Introduction to Boundary Layer Meteorology, Atmospheric and Oceanographic Sciences Library, Springer Dordrecht, Columbia, Vancouver, Canada, ISBN 978-94-009-3027-8, https://doi.org/https://doi.org/10.1007/978-94-009-3027-8, 1988.

Tang, L., Ramacher, M. O. P., Moldanová, J., Matthias, V., Karl, M., Johansson, L., Jalkanen, J. P., Yaramenka, K., Aulinger, A., and Gustafsson, M.: The impact of ship emissions on air quality and human health in the Gothenburg area – Part 1: 2012 emissions, Atmos. Chem. Phys., 20, 7509–7530, https://doi.org/10.5194/acp-20-7509-2020, aCP, 2020.

Thielicke, W., Hübert, W., Müller, U., Eggert, M., and Wilhelm, P.: Towards accurate and practical drone-based wind measurements with an ultrasonic anemometer, Atmos. Meas. Tech., 14, 1303–1318, https://doi.org/10.5194/amt-14-1303-2021, aMT, 2021.

Thompson, S. L., Yatavelli, R. L. N., Stark, H., Kimmel, J. R., Krechmer, J. E., Day, D. A., Hu, W., Isaacman-VanWertz, G., Yee, L., Goldstein, A. H., Khan, M. A. H., Holzinger, R., Kreisberg, N., Lopez-Hilfiker, F. D., Mohr, C., Thornton, J. A., Jayne, J. T., Canagaratna, M., Worsnop, D. R., and Jimenez, J. L.: Field intercomparison of the gas/particle partitioning of oxygenated organics during the Southern Oxidant and Aerosol Study (SOAS) in 2013, Aerosol Science and Technology, 51, 30–56, https://doi.org/10.1080/02786826.2016.1254719, doi: 10.1080/02786826.2016.1254719, 2017.

Thornton, J. A., Mohr, C., Schobesberger, S., D'Ambro, E. L., Lee, B. H., and Lopez-Hilfiker, F. D.: Evaluating Organic Aerosol Sources and Evolution with a Combined Molecular Composition and Volatility Framework Using the Filter Inlet for Gases and Aerosols (FIGAERO), Accounts of Chemical Research, 53, 1415–1426, https://doi.org/10.1021/acs.accounts.0c00259, doi: 10.1021/acs.accounts.0c00259, 2020.

Vandergrift, G. W., Dexheimer, D. N., Zhang, D., Cheng, Z., Lata, N. N., Rogers, M. M., Shrivastava, M., Zhang, J., Gaudet, B. J., Mei, F., and China, S.: Tethered balloon system and High-Resolution Mass Spectrometry Reveal Increased Organonitrates Aloft Compared to the Ground Level, Environmental Science & Technology, 58, 9909–10 414, https://doi.org/https://doi.org/10.1021/acs.est.4c02090, 2024.

von der Weiden, S.-L., Drewnick, F., and Borrmann, S.: Particle Loss Calculator – a new software tool for the assessment of the performance of aerosol inlet systems, Atmospheric Measurement Techniques, 2, 479–494, https://doi.org/10.5194/amt-2-479-2009, 2009.

Wu, C., Bell, D. M., Graham, E. L., Haslett, S., Riipinen, I., Baltensperger, U., Bertrand, A., Giannoukos, S., Schoonbaert, J., El Haddad, I., Prevot, A. S. H., Huang, W., and Mohr, C.: Photolytically induced changes in composition and volatility of biogenic secondary organic aerosol from nitrate radical oxidation during night-to-day transition, Atmos. Chem. Phys., 21, 14 907–14 925, https://doi.org/10.5194/acp-21-14907-2021, aCP, 2021.

Zhu, S., Ma, N., Yu, P., Xie, L., Hong, J., Lu, N., Bai, Z., Deng, Z., Ran, L., Wu, Y., Bian, J., Wang, Q., Tao, J., Zhou, Y., Wang, Q., Su, H., and Cheng, Y.: Vertical Profiling of Aerosol Physicochemical Properties With a New Airborne Aerosol Sampling System for Unmanned Aerial Vehicles and Tethered Balloons, Journal of Geophysical Research: Atmospheres, 130, e2024JD043 148, https://doi.org/https://doi.org/10.1029/2024JD043148, 2025.

Supporting Information: A drone-based sampling platform for vertically resolved chemical characterization of aerosol particles using chemical ionization mass spectrometry

Leo Håkansson[1], **Epameinondas Tsiligiannis**[1], **and Cheng Wu**[1]

[1]Department of Chemistry and Molecular Biology, University of Gothenburg, Sweden

Correspondence: Cheng Wu (cheng.wu@gu.se)

Table S1. Summary of measurements

Measurement	Height MAGL	Filter sampling time (h)	Description	Date
Hovering	8	3	Comparison of drone and ground-based while drone is hovering, simultaneous stationary and drone based sensor measurements	11 May 2025
Grounded	2	3	Comparison of drone and ground-based while drone is grounded	10 May 2025
Vertical profile test	2–120	–	Vertical profiles of T, RH, wind speed and direction between 19:30 and 02:30	24 Apr 2024
Nocturnal boundary layer profile	2–120	1.5	Vertical profiles of T, RH, wind speed and direction during the nocturnal boundary layer profiling, simultaneous ground and drone based filter collection	14-15 Apr 2025

Figure S1. Drone setup used in comparison measurements. On the left: Natrium Atmospheric and climate measurement tower.

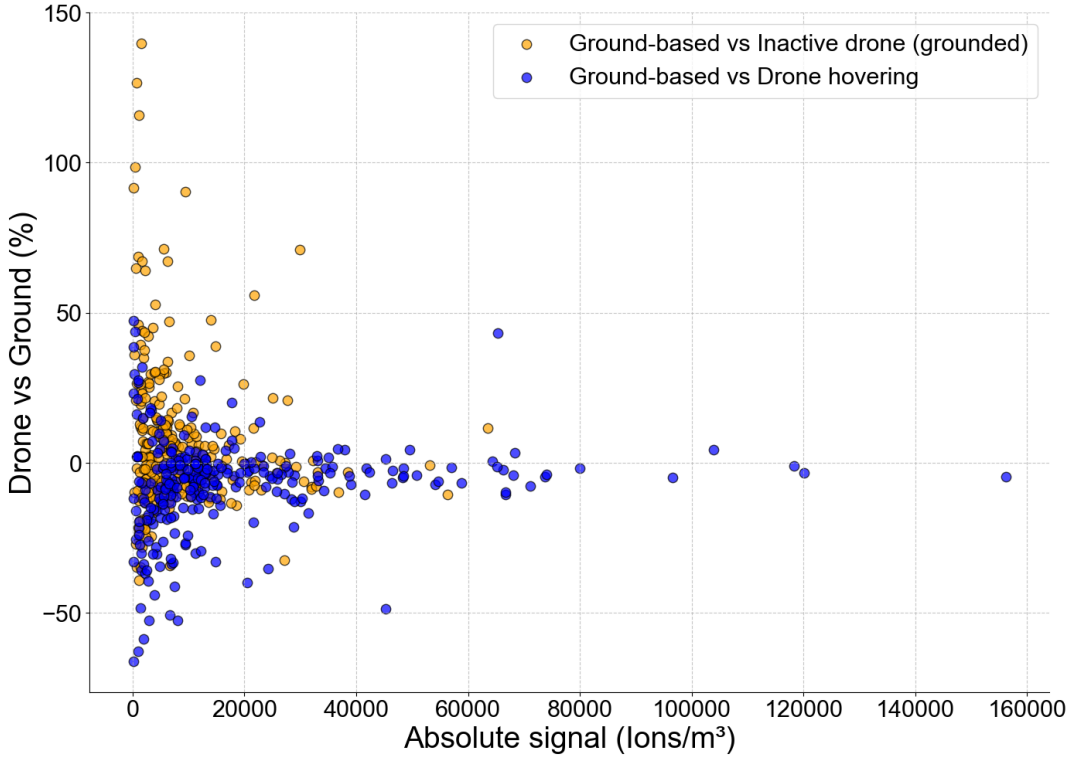

Figure S2. Distribution of relative difference between drone and ground-based measurements ((drone-ground)/ground) as a function of absolute signal of ground-based measurements.

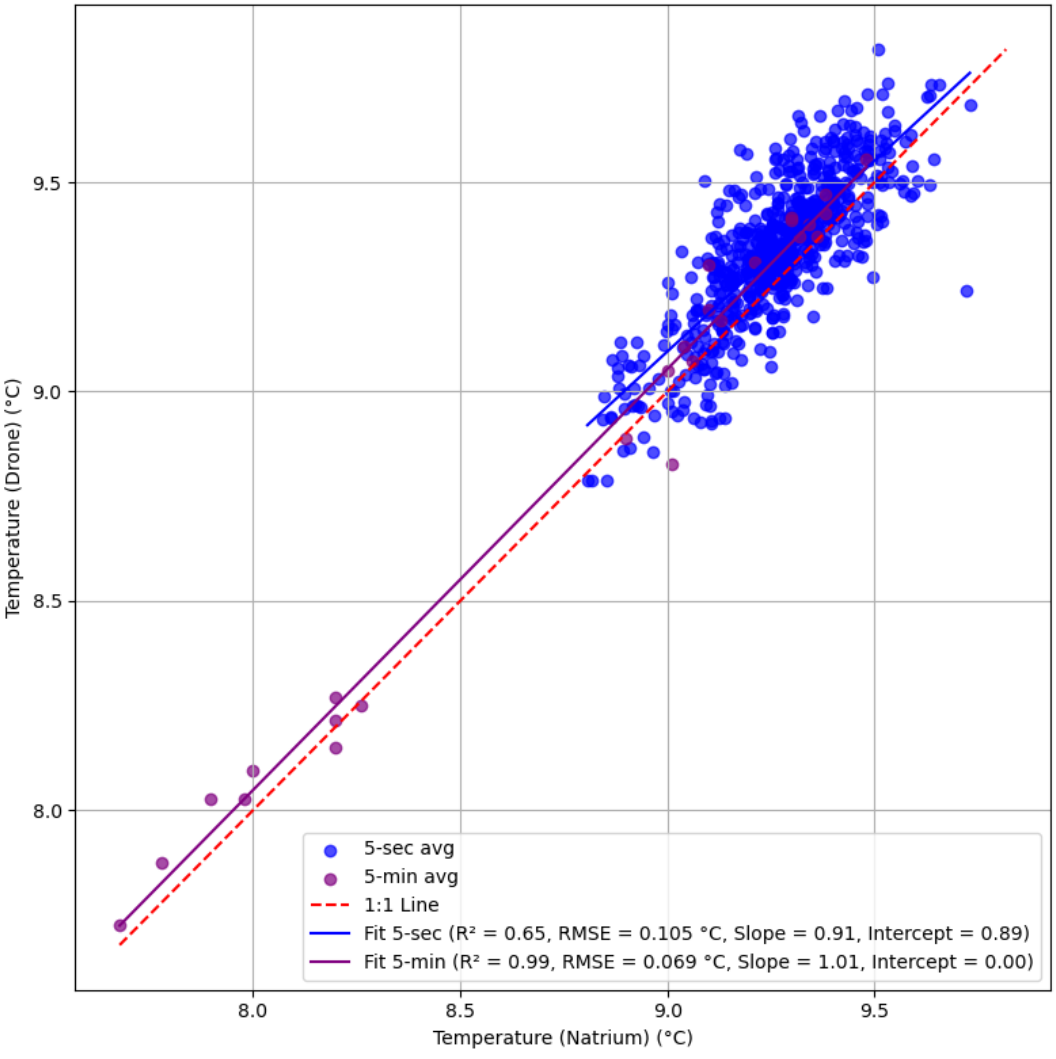

Figure S3. Temperature correlation plot between drone and ground-based (Natrium) measurements.

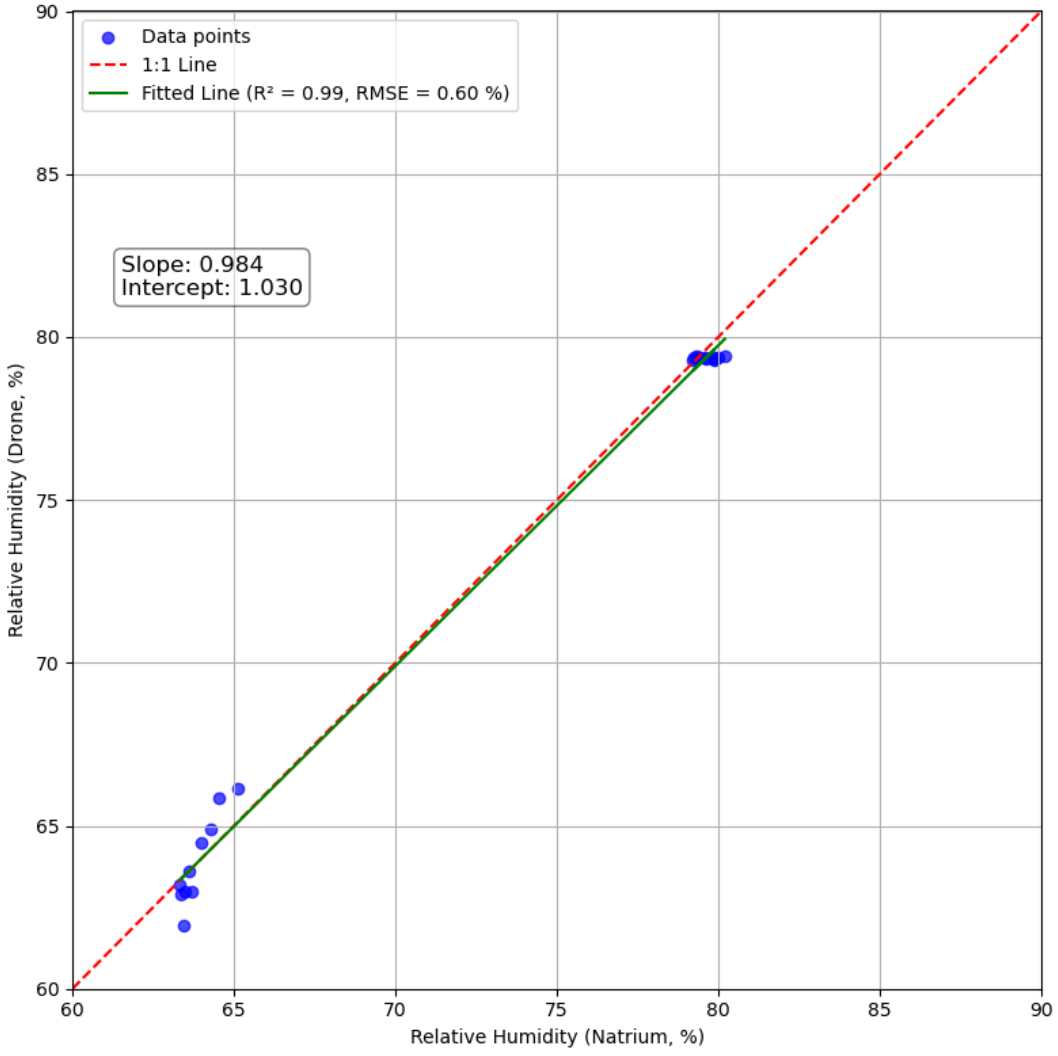

Figure S4. Relative humidity (RH) correlation plot between drone and ground-based (Natrium) measurements.